RSC Advances

ROYAL SOCIETY OF CHEMISTRY

www.rsc.org/advances

Journal Name

RSCPublishing

ARTICLE

Controllable preparation and properties of active functional hybrid materials with different chromophores

Cite this: DOI: 10.1039/x0xx00000x

Received 00th January 2012,
Accepted 00th January 2012

DOI: 10.1039/x0xx00000x

www.rsc.org/

Shizhe Wang,[a]Shanyi Guang,[b]Hongyao Xu,[a]* and Fuyou Ke[a]

A convenient and efficient strategy for preparing active functional hybrid materials was proposed based on the investigation of controllable preparation of a serial of anthracene-containing organic-inorganic functional hybrid materials with active ethylene group. These functional hybrid materials with different active vinyls were controllable prepared through Heck reaction with octavinylsilsequioxane (OV-POSS) as raw materials by adjusting the feed ratio. Their structures and properties are characterized and evaluated by various measurements The influence of molecular structure onoptical properties of resulting hybrids was investigated in detail. It was found that the incorporation of nano-sized inorganic polyhedral oligomericsilsesquioxane(POSS) can efficiently prevent aggregation of hybrid molecules owing to the prohibition of π-π stacking between chromophore groups, which is also confirmed by the theoretical simulation. Simultaneously, thermal gravimetric analysis (TGA) results also show that the inorganic POSSs make the hybrids possess good thermal stabilities.

Introduction

Organic-inorganic molecular hybrid nanocomposites are of great interest because they offer the potential to realize remarkable and complementary properties which cannot be obtained from a single material.[1-3] Polyhedral oligomericsilsesquoixanes (POSS) is a class of inorganic compounds with nano-scale dimensions (0.5~3 nm) and has a well-defined cubeoctameric structure with a silica-like core (Si_8O_{12}) surrounded by eight organic corner groups (functional or inert), which makes POSS molecules to be excellent platforms and blocks for nanotechnology applications and architecture of novel organic/inorganic hybrid nanocomposites.[4-6] More importantly, POSS molecules offer a unique opportunity for preparing organic/inorganic molecular hybrid with the inorganic structural units covalently incorporated and truly molecularly dispersed into resultant hybrids, which effectively overcomes the aggregation effect occurred in common hybrid composites based on physical mixture.[7-11] Thus, the POSS molecules with unique structure provide many possibilities and opportunities to tailor materials' properties.[12, 13] Many POSS-based hybrid nanocomposites with different architectures have been prepared such as linear or pendant type hybrids,[14-17] star type hybrids[18, 19] and network type hybrids[20-22] and their thermal properties and thermal enhanced mechanism[23, 24] were investigated. Various functional POSS-based materials were designed and reported. However, these works were mainly focused on design of single functional materials. With the development of technology and society, the requirement of multifunctional materials was proposed step by step.

In previous publications, reaction between the functional molecules and POSS is the typical path to get hybrid materials.[25-27] The hydrosilylation reaction is one of the widely used way to modify the POSS, but the structure is hard to be controlled when feed ratio more than 1:4.[28] And click is also a widely used method to prepare functional hybrid materials.[29-31] It is well known that OV-POSS is a commonly used material to prepare functional hybrid materials but the structure is difficult to be controlled.[32] The controllable preparation of OV-POSS hybrid materials is always a tough issue in this field. The key in solving the problem once lies on the controllable preparation of functional hybrid materials with active groups.

In the paper, a convenient and efficient strategy for preparing active functional hybrid materials (Ft-OV-POSS) were investigated by molecular design based on the study of controllable preparation of a serial of anthracene-containing organic-inorganic functional hybrid materials with active ethylene groups. These active functional hybrid materials will provide the important foundation for preparation of multifunctional hybrids materials in future.

Results and Discussion

Preparation of the hybrid materials

In this work, anthracene was selected as a luminescence and optical identification group, and ethylene groups as an active group. The active functional hybrid materials were designed and prepared using **OV-POSS** as a raw material to react with 9-bomoanthracene (**9-BA**) by typical Heck reaction.

The resulting hybrid materials with different numbers of active groups and functional groups were obtained by changing feed

ratio, using $Pd(Ac)_2$ and PPh_3 as the catalyst system and Et_3N as acid-binding agent. During the reaction, triethylamine hydrobromide precipitates were produced. The reaction degree can be conveniently observed and estimated based on the amount of the salt. All the products have good solubility in common solvents, such as THF, DCM, chloroform, toluene and ethyl acetate. When their solution were spin-coated on glass sheet, a uniform film can be formed (microscopic examination), which shows the very well film-forming ability of the resultant materials. Simultaneously, it was found that the yield of H1 is relatively low when the feed ratio of **9-BA** to OctaVinyl-POSS is 1:1 (molar ratio). The probable reason may be that the complex of palladium and **9-BA** is hard to form when the concentration of **9-BA** is low. However, when the feed ratio was increased to 2:1 and 10:1, the **H2** and **H3** were obtained in moderate yield, respectively.

Characterization and discussion

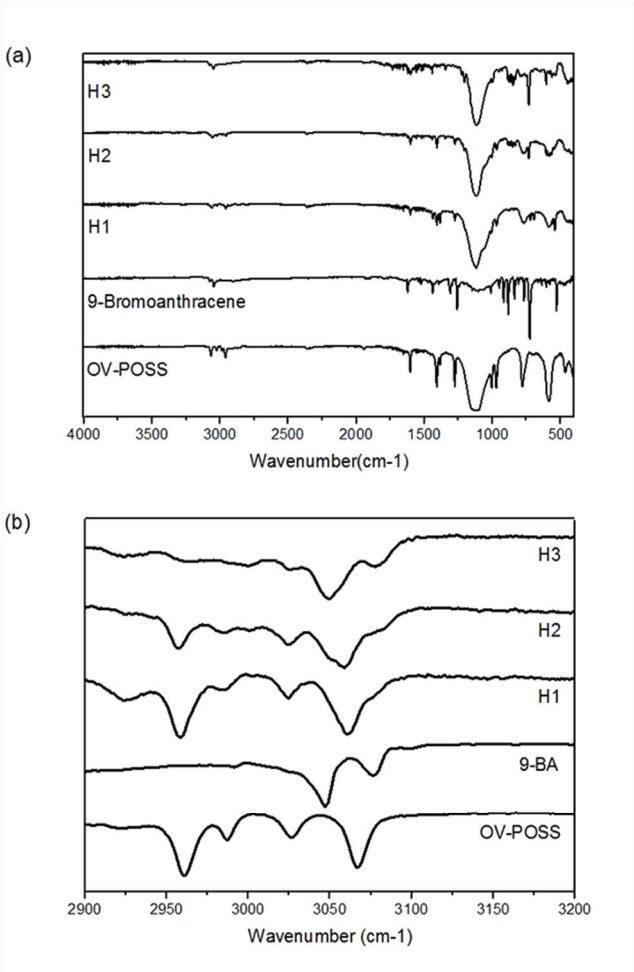

Fig.1 The FTIR spectra of **OV-POSS**, **9-BA**, **H1**, **H2**, **H3** (a) andthe magnification spectra between 2900 and 3200 cm^{-1} (b).

FTIR analysis Fig.1 (a) shows the FTIR spectra of the **OV-POSS**, **9-BA** and the hybrid materials. Obviously, the existence of the peaks at 1118 cm^{-1} (Si-O-Si stretching) in all the hybrid materials' spectra means the presence of POSS core. On the other hand, the peaks representing anthryl group at 3075, 3048 (Ar-H stretching), 1622, 1440 (Ar stretching) and 727 cm^{-1}(C-H bending) can also be seen in the hybrid materials' spectra, which prove the incorporation of anthryl into the resulting hybrids. Furthermore, the peaks at 3065, 3027, 2987 and 2961 cm^{-1}gradually fade out with increase of feed ratio and the peaks at 3075 and 3048 cm^{-1} displayed a more and more clear pattern in the magnification of the IR spectra between 2900 and 3200 cm^{-1}(**Fig.1 (b)**), clearly revealing the growth of the average substituted number from **H1** to **H3**.

Fig.2 ^{1}H-NMR spectra of **OV-POSS**, **H1**, **H2**, **H3** (a) in $CDCl_3$

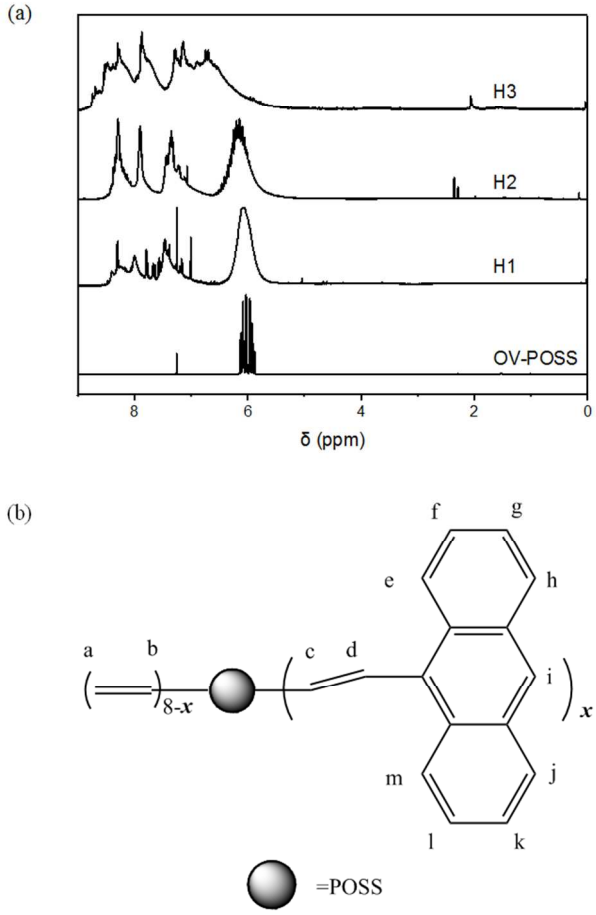

and location mark of hydrogen atom in hybrid molecule (b).

^{1}H-NMR analysis The ^{1}H-NMR tests were carried out and the results were shown in **Fig.2 (a)**. The peaks at 6.0 ppm in ^{1}H-NMR spectra represent the hydrogen atoms on unreacted ethenyls (H **a-b,** 3 × (8 –***x***)) and the hydrogen atoms on reacted ehtenyls which are near to POSS (H **c,*x***) and the peaks above 6.5 ppm represent all hydrogen atoms on anthryls and the hydrogen atoms on reacted ehtenyls which are near to anthryls (H d-m, 10 ***x***) in **Fig.2 (b)**.On the other hand, the ratio of the area above 6.5 ppm to the area around 6.0 ppm which can be obtained by integrating the area of peak in the ^{1}H-NMR spectra, and this ratio is recorded as ***r***. As the ratio (**r**) and the expression of the hydrogen atoms were all obtained, the average substituted number (***x***) of the hybrid materials can be calculated approximately by **Equation.1**:

$$10\,x / (3 \times (8 - x) + x) = r \quad \text{(Equation.1)}$$

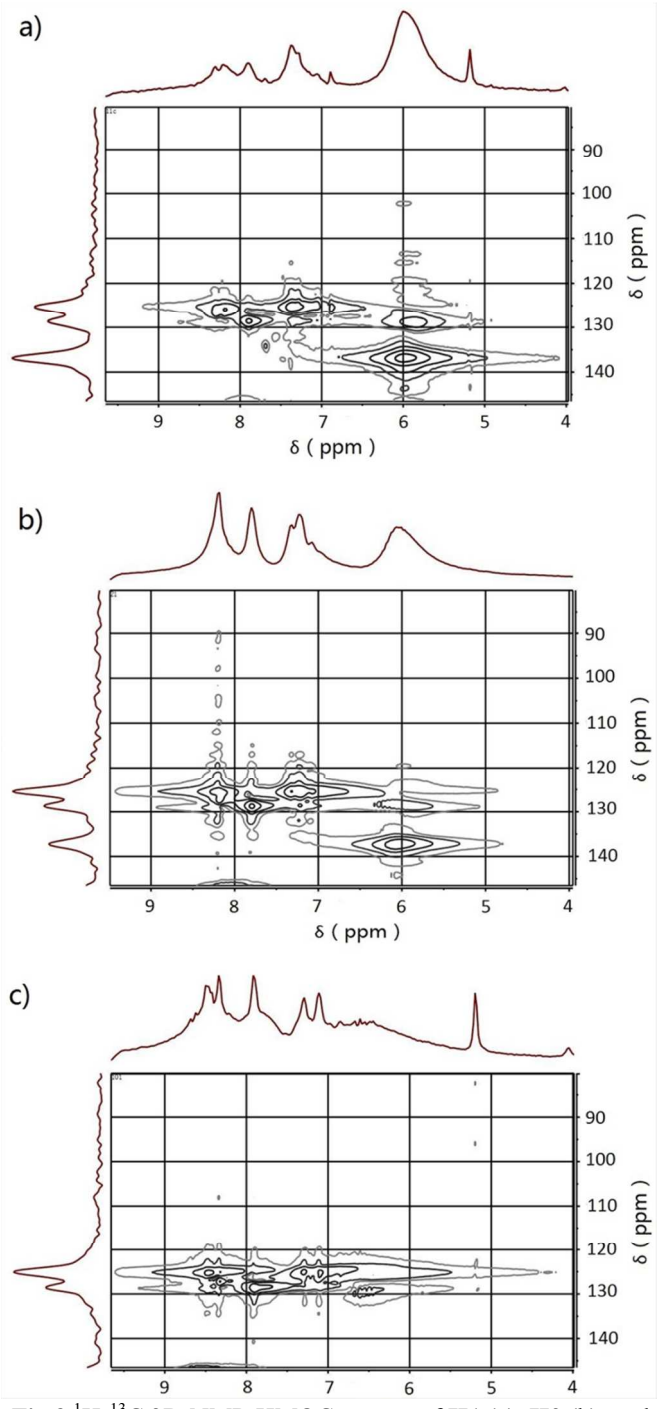

Fig.3 ^{1}H-^{13}C 2D-NMR HMQC spectra of **H1** (a), **H2** (b), and **H3** (c) in $CDCl_3$.

The calculated results from ^{1}H-NMR spectra reveal that the average functional group number (***x***) of **H1** and **H2**to be 1.3 and 2.7 respectively. However, as no obvious peak existed in the spectrum of **H3** at 6.0 ppm, it can be said that almost all ethenyls had reacted in **H3**. Moreover, the peaks of anthryls in the spectra of**H2** and **H3** show a slight shift to high-field region, this may be attributed to T-shape interaction which caused by the shielding effect of the electron cloud of aromatic rings to the hydrogen atoms when the distances between them are close enough.[33]

Table.1 ^{1}H-^{13}C 2D-NMR HMQC data of **H1**, **H2** and **H3**.

Position*	Sample					
	H1		**H2**		**H3**	
	δH	δC	δH	δC	δH	δC
a,b,c	6.0	136.8	6.0	137.4	-	-
d	5.9	128.8	6.0	128.4	5.9	129.0
	-	-	-	-	6.4	129.3
Anthryl	8.2	126.0	8.2	125.5	8.4	125.2
	7.9	128.6	7.8	128.7	7.9	128.5
	-	-	-	-	8.3	127.3
	7.4	125.3	7.2	125.3	7.3	128.1
	-	-	7.2	125.4	7.1	125.2

*The position was displayed in **Fig.2 (b)**.

HMQC 2D-NMR analysis To further confirm the conclusion above, we carried out the 2D-NMR HMQC spectra of **H1**, **H2** and **H3** which were shown in **Fig.3**, and the data were summarized in **Table.1**. Apparently, the spectra of **H1** and **H2** have obvious peaks relate to the unreacted ethenyls (δH 6.0, δC 136.8 137.4), but these peaks did not appear in **H3**'s spectrum, which further supports that almost all the ethenyls had reacted in **H3**. This is consistent with the results of ^{1}H-NMR spectra. Furthermore, the peaks around δH 5.9-6.5 ppm, δC 129.0 ppm shifted to low-field region from **H1** to **H3** which have revealed the disappearance of unreacted ethenyls. And this shift is also coincident with the result of ^{1}H-NMR and explicates the why the peak at 6.0 ppm of **H2** have a slight shift to low-field in ^{1}H-NMR.

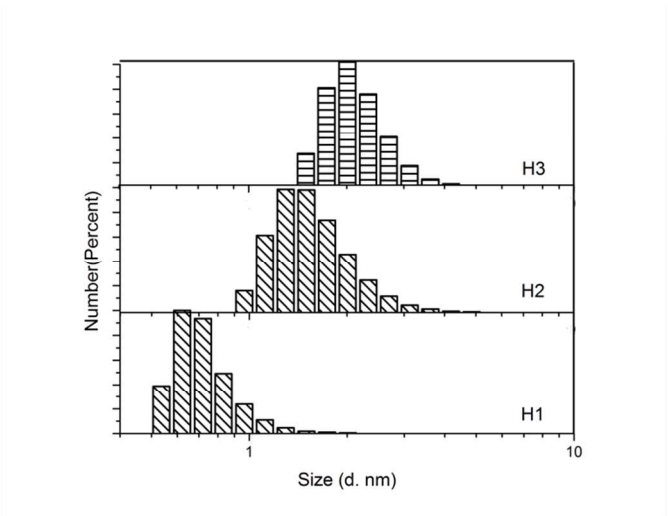

Fig.4 Particle size distribution of **H1**, **H2**, and **H3** in toluene with a concentration of 1 $g \cdot L^{-1}$

Particle size analysis In fact, it is difficult to show real molecular structure using the particle size distribution measurement owing to laser scattering error of asymmetric molecules and strong optical absorption of asymmetric hybrid molecules. However, the average particle size can also indirectly reflect the structure of the resulting hybrid molecules. Thus, the particle size tests were carried out. The results were shown in **Fig.4**. From **Fig.4**, it can be easily seen that the average diameter of **H1** is the smallest and **H3** is the largest.

Table.2 the chromophore ratio results calculated from ^{1}H-NMR and UV-vis spectra

Sample	Feed Ratio	Reacted Ethenyls (r)[a]	Theoretical Chromophores in certain mass [b](mol)	Ratio[c]	UV-vis Absorption	Ratio[d]
H1	1:1	1.3	1.48×10^{-5}	100	0.181	100
H2	2:1	2.7	2.43×10^{-5}	164	0.305	168
H3	10:1	8.0	3.92×10^{-5}	264	0.467	258

a. calculated from ^{1}H-NMR and 2D-NMR.
b. use equation ***m*** / ***M*** * ***x*** to calculate, ***m*** = 10 mg, ***M*** = 633+177 * ***x***, ***m*** is the mass of the hybrid materials, ***x***is the calculated average substituted number of **H1**, **H2** and **H3**; ***M*** is the average molecule weight of the hybrid materials.
c. take the theoretical chomophores in certain mass of **H1** as 100%
d. take the UV-vis absorption of **H1** at 373 nm as 100%

Undoubtedly, bigger size means more anthryls in one molecule. **UV-vis spectra analysis Fig.5** shows the UV-vis spectra of the hybrid materials **H1**, **H2**, and **H3**. It can be seen that the absorption intensity of peak at 372 nm corresponding to anthryl merit increases with the feed ratio, demonstrating the higher feed ratio leads to more anthryls incorporated into hybrid molecules. The peak at 372 nm in these hybrids with more anthryl group displays a slight red shift of ca. 1-2 nm, which may be attributed to the interaction between the function groups. However, the normalized curves (upper right inserted plate) had little difference in pattern, revealing that they have almost the same molecular structure, further supporting that the OV-POSS may mainly show single-substituted structure.

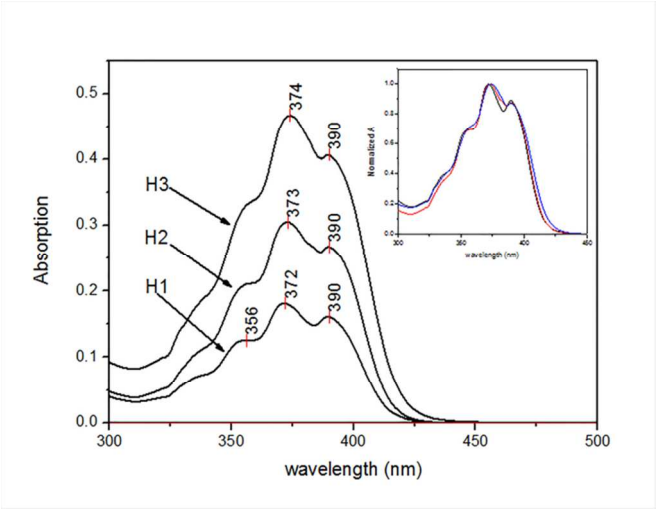

Fig.5 The UV-vis spectra of **H1**, **H2**, **H3** in toluene(1×10^{-2} g·L^{-1}). Inset: The normalized spectra

The theoretical amount of chromophores(***N*** / mol)in certain mass of hybrid materials can be calculated through the average reacted ethenyls number of the hybrid materials (***x***,the average substituted number was calculated from ^{1}H-NMR results) by **Equation.2** and **Equation.3.**

$$M = 633 + 177 \times x \quad \text{.....Equation.2}$$

$$N = x \times m / M \quad \text{.....Equation.3}$$

Equation.2is used to calculate the average molecular weight , where 633 and 177are the molecular weights of **OV-POSS** and anthryl group, respectively. And (633 + 177 × ***x***) is the average molecular weights(***M*** / g·mol^{-1}) of different hybrid materials when ***x*** = 1.3, 2.7 and 8.0. When the average molecular weights of the hybrid materials were got, the amount of molecules in certain mass (***n***) could be calculated as ***m*** / ***M*** in **equation.3**, where ***m*** (10mg) was the mass of the hybrid materials. In order to compare with the results of UV-vis spectra, the theoretical chromophores amount (***N***) should be get by multiplying the amount of molecules (***n***) by ***x***, which is showed in **Equation.3**.As showed in **Table.3**, the theoretical ratio of the amount of chromophores (***N***) in certain mass of **H1**, **H2**, **H3** was 100 : 164 : 264, which were calculated from ^{1}H-NMR. According to Lambert-Beer Law, the absorption (Abs) of the UV-vis spectrum is positively proportional to the amount of the chromophores, so the UV-vis absorption intensity of the hybrid materials can reflect the ratio of the amount of chormophores in the solution. For comparison, the solutions with same mass concentration were prepared for the measurement of UV-vis spectra. In this solution, absorption intensity of **H1** was taken as 100%, and that of **H2** and **H3** were 168% and 258% respectively, which hints the ratio of UV-vis absorption of **H1**, **H2** and **H3** to be 100 : 168 : 258. The similarity of two ratios reveal the consistency of the structures of the hybrid materials. In addition, the linear region of the instrument is 0.1-2.8 which promise the precise of the result.

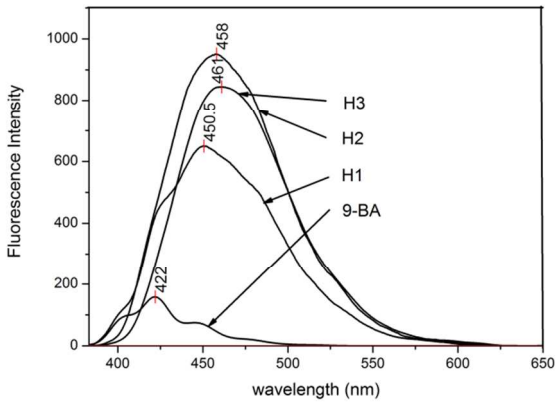

Fig.6 The PL spectra of **9-BA**, **H1**, **H2**, and **H3** in toluene. Excitation wavelength: 373 nm, (2×10^{-2} g·L^{-1}).

PL spectra analysis In order to understand the interaction between the functional groups in single molecule, solution PL spectra were performed and the results were displayed in **Fig.6**. The emitting peaks of **9-BA**, **H1**, **H2** and **H3** were located at 422 nm, 451 nm, 458 nm and 461 nm respectively. **9-BA** shows more precise peaks and the resulting hybrids with more anthryls show obvious red shift owning to the incorporation of ethylenes, *J*-aggregation and *T*-shape interaction of anthryls in hybrid molecules. In addition, the intensity of the PL spectra of hybrids was in the order of **H2**>**H3**>**H1**> **9-BA** at same mass concentration. Apparently, solution of **H3** has highest chromophores concentration but its PL intensity is lower than **H2**'s, on the other side, **H2**'s PL intensity is 141% of **H1**'s, which is not corresponding to the UV-vis spectra result of 100 : 164 It can be supposed from the intensity between **H2** and **H1**

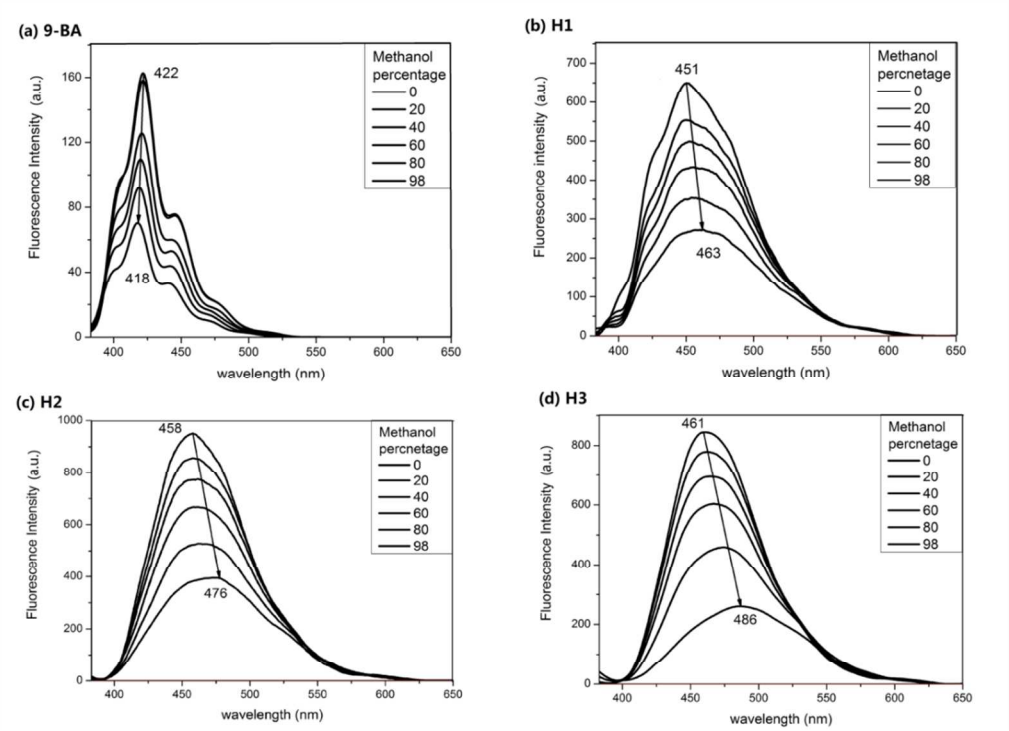

Fig.7 The PL spectra of **9-BA** (a), **H1**(b), **H2**(c), and **H3**(d) with different percentage of poor solvent. (Excitation wavelength: 373 nm; 2×10^{-2} g·L^{-1}; 0, 20, 40, 60, 80, 98 vol% of methanol in toluene-- from top to bottom)

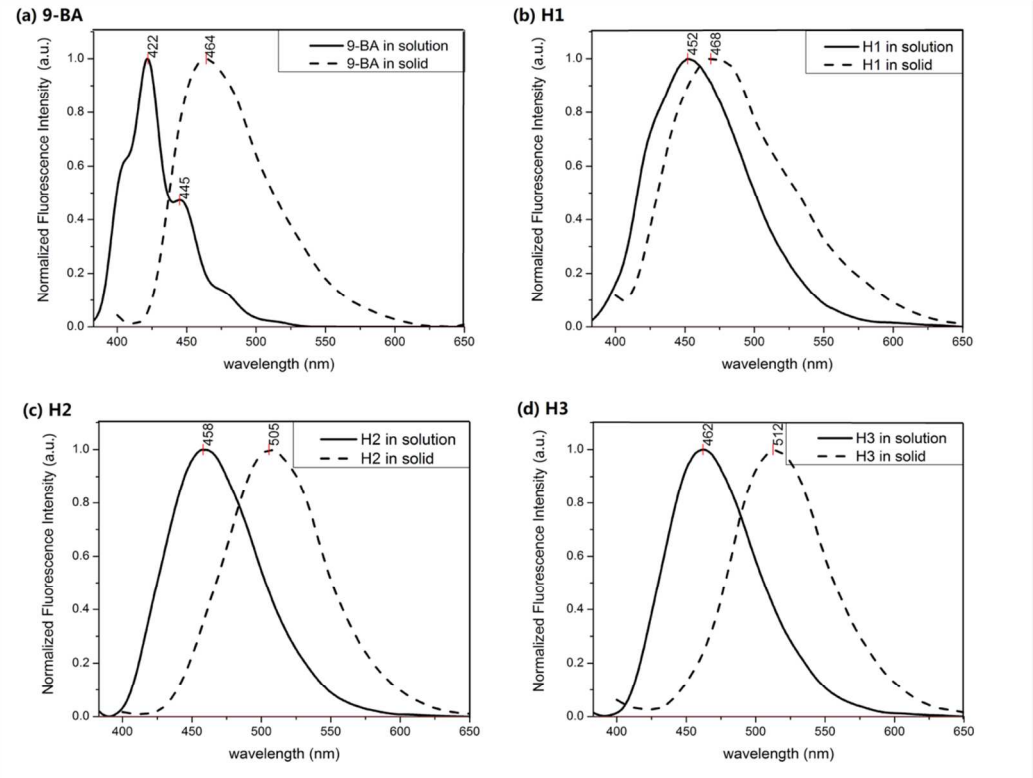

Fig.8 Normalized PL spectra of **9-BA** (a), **H1** (b), **H2** (c), and **H3** (d) in solution (Excitation wavelength: 373 nm; 2×10^{-2} **g**·L^{-1}) and solid state film (Excitation wavelength: 373 nm; opaque film).

That these functional groups prefer to substitute on the position with less steric hindrance when there are less anthryls in the molecule but the interaction between anthryl groups in H2 is still inevitable. However, when there are more anthryls, the aggregation and interaction is much stronger, *J*-aggregation and *T*-shape interaction not only lead to red shift but also the decrease of fluorescence intensity.[33, 34]

The mixture solvent (toluene as good solvent and methanol as poor solvent) was used to explore the relationship between molecular structure and the aggregation effect of hybrid molecules, the results were showed in **Fig.7**.With the increasing percentage of methanol, **9-BA** showed a blue shift but the hybrid materials showed red shift. This phenomenon revealed the incorporation of POSS had changed the π-π stacking H-aggregation of the organic group into J-aggregation and dipole-dipole interaction. Moreover, the red shift of H1, H2 and H3 were 12 nm, 18 nm and 25nm respectively. Obviously, if there are more anthryls in the molecules, the stronger interaction between the chromophores will lead to more red shift. H3 showed largest red shift, which hinted it had largest substituted number, this is corresponding with the results from the FTIR and ^{1}H-NMR spectra.

Owing the well film-forming ability of these hybrids, to further study the aggregation behaviors of the hybrid materials, solid state PL spectra were carried out and the results were shown in **Fig.8**. It can be noticed that the PL spectra of **H1**, **H2** and **H3** in solid state have a further red shift from 451 to 468 nm for **H1** with $\Delta\lambda$ = 17 nm, from 458 to 505 nm for **H2** with $\Delta\lambda$ = 47 nm, and from 461 to 512 nm with $\Delta\lambda$ = 51 nm. Interestingly, **9-BA** showed a red shift from 422 to 464 nm with $\Delta\lambda$ = 42 nm. The results reveal the fact that **H1** had the lowest aggregation effect but **H2** and **H3** still aggregate strongly, which is in agreement to the result above and our previous work.[22, 26, 34, 35] and also prove the guess that more anthryls promote the interaction between the chromophores.

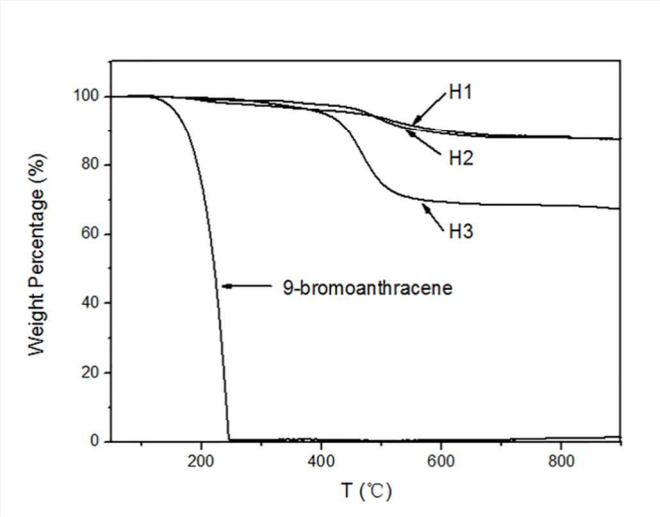

Fig.9 TGA curves of **9-BA**, **H1**, **H2**, and **H3**from r.t. to 900℃ in N_2 ramp of 10 mL·min^{-1}

Thermal stability Fig.9 shows the thermal properties of these hybrids. In **Fig.10**, we found **9-BA** had all decomposed at 246 ℃, but the thermal decomposition temperature (T_d, 5wt% loss) of **H1**, **H2** and **H3** were 468 ℃, 480 ℃, and 407 ℃, respectively, which hints that the resulting hybrids show very high thermal stability. This may mainly attributed to thermal hindrance of inorganic POSS core that possesses high thermal properties.[7, 25, 28, 36, 37] **E**ven at 900℃, total weight loss of them were only 12.5%, 12.4% and 32.5% for **H1**, **H2** and **H3**, respectively, which accounts for only 24.1%, 19.8% and 40% of the theoretical value.

Theoretical simulation In order to understand the interaction behaviors of the anthryls in the hybrid materials, theoretical simulations were carried out. The structure of the hybrids was optimized with the method DFT B3LYP/6-31G(d) on Gaussian09 software. Six kinds of molecular models were chosen for the optimization. **Fig.10** shows the molecular models: **M2** has two anthryls on body diagonal position; **M3** and **M4** three and four anthryls at face diagonal position each other; **M5** has one more anthryl than **M4**; **M8** has 8 anthryls on every ethenyls and **M2o** has two anthryls on the neighbouring position. The corresponding band gap ($\mathbf{E_g}$) and distance of different group in hybrid molecules to different substituted hybrids were summarized in **Talbe.3**. (The shortest distances between anthryls in single molecule were defined as the nearest distance between two carbon atoms on different anthryls.)

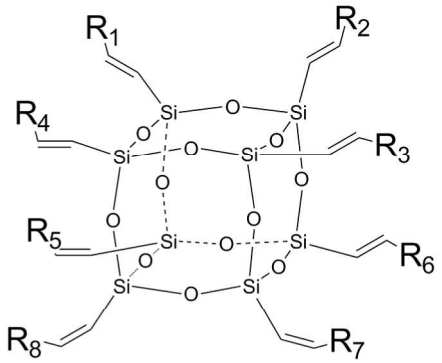

M2 R1,7 = Anthryl Others = H
M3 R1,3,6 = Anthryl Others = H
M4 R1,3,6,8 = Anthryl Others = H
M5 R1,2,3,6,8 = Anthryl Others = H
M8 R1-8 = Anthryl
M2o R1,2 = Athryl Others = H

Fig.10 Models for theoretical simulation with different substituted position.

Table.3 Substituted position and the theoretical simulation results of band gap ($\mathbf{E_g}$) and Shortest distance between anthryls in single molecule.

No.	Substituted position	Band gap $\mathbf{E_g}$ (eV)	Shortest distanced between anthryls in single molecule (Å)
M2	1,7	3.404	13.620
M3	1,3,6	3.373	8.537
M4	1,3,6,8	3.345	7.685
M5	1,2,3,6,8	3.361	4.181
M8	All	3.233	3.850
M2o	1,2	3.268	4.180

According to the simulation results in **Table.3**, E_g and the intramolecular distance between anthryls decreased with the increase of substituted number. Apparently, lower E_g means low energy which is consistent with the red shift of PL spectra. The shorter the intramolecular distance between anthryls hints the higher intramolecular interaction which is corresponding with the red shift in solution PL spectra. In order to illustrate the influence of the substituted position on intramolecular group interaction, two ortho-position substituted model (**M2o**) was also chosen in the simulation. The results reveal that the shortest distance between two carbon atoms in two anthryls is at ca. 4.180 nm when two functional groups are located at this position. Based on previous report, a strong interaction will happen.[22, 38] In addition, in **M8**, the arrangement of anthryls benefitting *J*-aggregation and *T*-shape interaction which is coincident with the red shift of PL spectra from **H1** to **H3.**

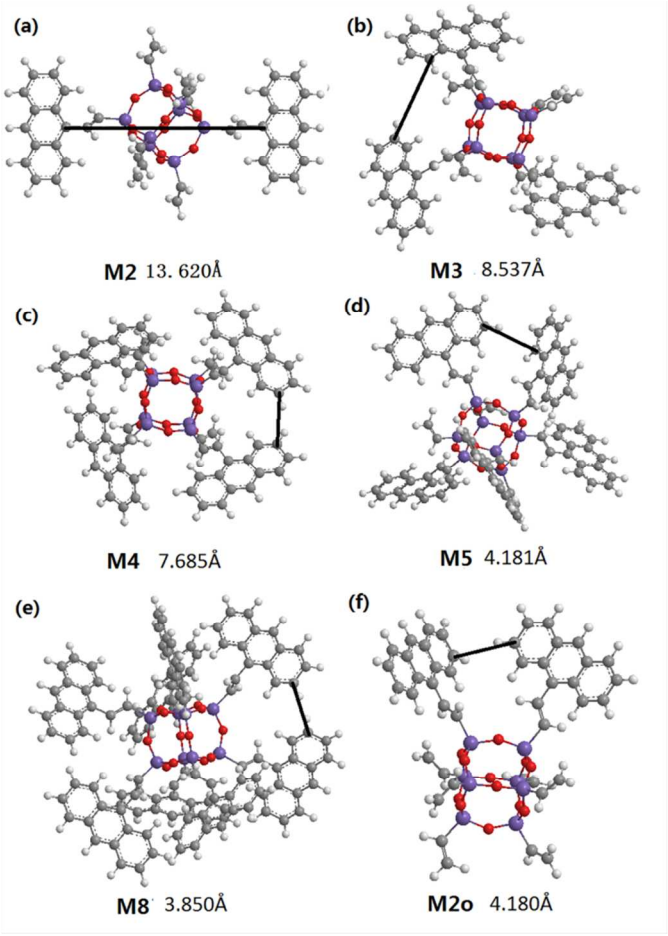

Fig.11 Optimization results of model **M2**, **M3**, **M4**, **M5**, **M8** and **M2o** and their smallest distance between anthryls (shortest distances of two carbon atoms in different anthryls).

Finally, the aggregation behaviour of the dimmers of the hybrid materials with one function groups was optimized and the results were shown in **Fig.12**. **Fig.12 (a)** displays the optimized result start from face to face position. Obviously, the shortest distance between two anthryls was 5.213 Å and the dihedral angle was 55°, which illustrate the interaction between anthryls was very weak[33, 39] and resulted in the minimal red shift of **H1**'s PL spectra between solution and solid state. On the other hand, the optimized result of dimmer start from head to head type showed a smaller shortest distance (4.056 Å) and dihedral angle of 52°,which implies the interaction between anthryls was stronger. In **Fig.12 (b)**, it can be observed that the anthryls overlapped slightly and took an untypical *J*-aggregation. Besides, the shortest distance of proton on one anthryl to the surface of the other anthryl is 3.146 Å, provided the evidence of the existence of *T*-shape interaction.[33] In summary, hybrids with less anthryls show almost no intra-molecules interaction and less aggregation in condensed state, but hybrids with more anthryls will display both intra-molecule interaction and inter-molecule interaction which lead to more red shift and decrease of the PL intensity.

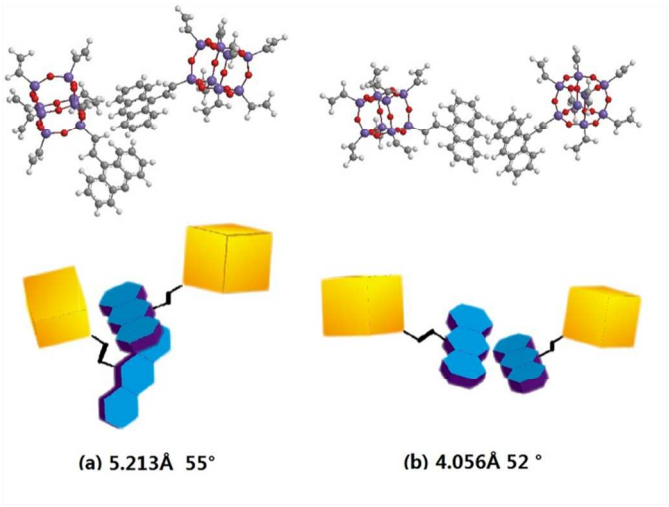

Fig.12 Optimization results of dimmers start from face to face (a) and head to head (b) position.

Experimental

Synthetic procedures

The hybrids were prepared with typical Heck reaction. The reactions were carried out in nitrogen atmosphere with a vacuum-line system. And **H1** was taken as an example: 2.532 g (4 mmol) **OV-POSS**, 1.028 g (4 mmol) 9-bromoanthracene, 0.045 g (0.2 mmol, 5 mol% of 9-bromoanthracene) $Pd(Ac)_2$ and 0.210 g (0.8 mmol, 20 mol% of 9-bromoanthracene) PPh_3 were added to a 200 mL schlenk flask, vacuum-nitrogen three times to keep an inert atmosphere, 30 mL toluene and 10 mL Et3N added and stirred for 12 h in room temperature, then heated to 80℃ to react for 48 h, and brown solution and white precipitate were observed. The solution was cooled down to room temperature and then filtered through 1 cm Celite. The solution was rotary evaporated. The product was obtained and purified by column chromatography with CH_2Cl_2/petroleum ether as eluting agent.

H1, brown transparent solid was obtained in yield 23.6%. FTIR (KBr), ν (cm^{-1}): 3061, 3024, 2985, 2957 (Si-CH=CH2), 1623, 1442 (Ar), 1602 (Si-CH=CH2), 1123 (Si–O–Si), 722 (Ar-H). 2D-NMR HMQC: ^{1}H-NMR (400 MHz, $CDCl_3$), δ, (ppm): 6.01(br, Si-CH=CH2), 7.40, 7.92, 8.24 (br, Ar–H); ^{13}C-NMR (100.13 MHz, $CDCl_3$), δ, (ppm):125.15, 128.94 (Ar-H, Si-CH=CH-Ar), 136.92 (Si-CH=CH2). ^{29}Si-NMR (79.49 MHz), δ, (ppm): -80.17,-79.52 (Si-CH=CH2), -78.93 (Si-CH=CH-Ar)

The preparation processes of **H2** and **H3** were similar to **H1** with feed ratio of 2:1 and 10:1, respectively.

H2, brown transparent solid was obtained in yield 57.5%. FTIR (KBr), ν(cm^{-1}): 3059, 3023, 2984, 2958 (Si-CH=CH2), 3048 (Ar-H), 1623, 1442 (Ar), 1602 (Si-CH=CH2), 1123 (Si–O–Si), 732 (Ar-H). 2D-NMR HMQC: ^{1}H-NMR (400 MHz, $CDCl_3$), δ,

(ppm): 6.08 (br, Si-CH=CH2), 7.23, 7.79, 8.18 (br, Ar–H); ^{13}C-NMR (100.13 MHz, $CDCl_3$), δ, (ppm): 125.46, 128.47 (Ar-H, Si-CH=CH-Ar), 137.14 (Si-CH=CH2). ^{29}Si-NMR (79.49 MHz), δ, (ppm): -79.59 (Si-CH=CH2), -78.86 (Si-CH=CH-Ar

H3, brown transparent solid was obtained in yield 68.3%. FTIR (KBr),ν(cm^{-1}): 3061, 3027, 3048 (Si-CH=CH2, Ar-H), 1623, 1442 (Ar), 1602 (Si-CH=CH2), 1123 (Si–O–Si), 732 (Ar-H). 2D-NMR HMQC: ^{1}H-NMR (400 MHz, $CDCl_3$), δ, (ppm): 6.50 (br, Si-CH=CH-Ar), 7.23, 7.79, 8.18 (br, Ar–H); ^{13}C-NMR (100.13 MHz, $CDCl_3$), δ, (ppm): 125.15, 128.55 (Ar-H, Si-CH=CH-Ar). ^{29}Si-NMR (79.49 MHz), δ, (ppm): 79.13 (Si-CH=CH-Ar)

Materialsand methods

Octavinylsilsequioxane was purchased from AMWEST TECHNOLOGY COMPANY, Palladinum acetate and Triphenylphosphinewere purchased from Sinopharm Chemical Reagent Co., Ltd, 9-bromoanthracene was purchased from Shanghai Jiachen Chemical Co., Ltd. All solvents were AR commercial product, but toluene and triethylamine were purified before used.

FTIR spectra were measured with a Nicolet NEXUS 8700 FTIR spectrophotometer using KBr powder at room temperature.^{1}H-NMR and 2D-NMR HMQC spectra were recorded on a Bruker AVANCE/DMX 300.^{29}Si NMR spectra were recorded on a Bruker DMX-400 spectrometer. UV-vis spectra were recorded on a Lambda 35UV/Vis spectrometer (Perkin Elmer Precisely) using a 1 cm square quartz cell in toluene with a concentration of 10^{-2} g/L.PL spectra in solvent were recorded on a LS55 fluorescence spectrometer (Perkin Elmer Precisely) using a 1 cm square quartz cell and the excitation wavelength was 373 nm in toluene and mixture solvent of toluene/methanol with a concentration of 2×10^{-2} g/L, solid PL spectra were recorded on the same instrument with a opaque film on 1 mm quartz cell. Thermo gravimetric analyses (TGA) were carried out using a NRTZSCH TG 209F1 with a heating rate of 10 ℃/min from 25 to 900 □under a continuous nitrogen purge. Particle size testes were carried out using Nano ZS Particle Size & Zeta Potential Analyzer (Malvern) in toluene with a concentration of 1 g/L.

Conclusions

In conclusion, the hybrids with different active functional group can be synthesized controllable by changing the feed ratio easily, which will provides an important platform for preparation of multifunctional hybrid materials in future. The incorporation of POSS into hybrids can effectively prohibit the optical aggregation between optical chromophores. Simultaneously, it is found that these resultant hybrids possess very well thermal stability.

Acknowledgements

This work is financially supported by National Natural Science Fund of China (Grant Nos. 21271040, 21171034 and 51073031),Shanghai Youth Natural Science Foundation (12ZR1440100), “Chen Guang” project supported by Shanghai Municipal Education Commission, Shanghai Education Development Foundation (12CG37) and the Fundamental Research Funds for the Central Universities (12D10603).

Notes and references

[a]College of Material Science and Engineering & State Key Laboratory for Modification of Chemical Fibers and Polymer Materials, Donghua University, Shanghai 201620, P. R. China.
[b]School of Chemistry and Bioengineering, Donghua University, Shanghai, 201620, China.

1. J. Miyake and Y. Chujo, *Journal of Polymer Science Part A: Polymer Chemistry*, 2008, **46**, 6035-6040.
2. E. Gungor, C. Bilir, G. Hizal and U. Tunca, *J Polym Sci Pol Chem*, 2010, **48**, 4835-4841.
3. T. C. Lin, Y. H. Lee, C. Y. Liu, B. R. Huang, M. Y. Tsai, Y. J. Huang, J. H. Lin, Y. K. Shen and C. Y. Wu, *Chemistry*, 2013, **19**, 749-760.
4. H. Araki and K. Naka, *Journal of Polymer Science Part A: Polymer Chemistry*, 2012, **50**, 4170-4181.
5. B. Yu, X. Jiang and J. Yin, *Macromolecules*, 2012, **45**, 7135-7142.
6. M. Vielhauer, P. J. Lutz, G. Reiter and R. Mülhaupt, *Journal of Polymer Science Part A: Polymer Chemistry*, 2013, **51**, 947-953.
7. X. Su, S. Guang, H. Xu, X. Liu, S. Li, X. Wang, Y. Deng and P. Wang, *Macromolecules*, 2009, **42**, 8969-8976.
8. K. Kinashi, Y. Kambe, M. Misaki, Y. Koshiba, K. Ishida and Y. Ueda, *Journal of Polymer Science Part A: Polymer Chemistry*, 2012, **50**, 5107-5114.
9. N. Naga, T. Miyanaga and H. Furukawa, *Polymer*, 2010, **51**, 5095-5099.
10. K. Tanaka and Y. Chujo, *Journal of Materials Chemistry*, 2012, **22**, 1733.
11. X. Su, S. Guang, H. Xu, J. Yang and Y. Song, *Dyes and Pigments*, 2010, **87**, 69-75.
12. K. Yue, C. Liu, K. Guo, X. Yu, M. Huang, Y. Li, C. Wesdemiotis, S. Z. D. Cheng and W.-B. Zhang, *Macromolecules*, 2012, **45**, 8126-8134.
13. Y. Wang, A. Vaneski, H. Yang, S. Gupta, F. Hetsch, S. V. Kershaw, W. Y. Teoh, H. Li and A. L. Rogach, *The Journal of Physical Chemistry C*, 2013, **117**, 1857-1862.
14. F. Du, J. Tian, H. Wang, B. Liu, B. Jin and R. Bai, *Macromolecules*, 2012, **45**, 3086-3093.
15. J. Miyake, T. Sawamura, K. Kokado and Y. Chujo, *Macromolecular rapid communications*, 2009, **30**, 1559-1563.
16. X. Yang, J. D. Froehlich, H. S. Chae, S. Li, A. Mochizuki and G. E. Jabbour, *Advanced Functional Materials*, 2009, **19**, 2623-2629.
17. U. Kürüm, T. Ceyhan, A. Elmali and Ö. Bekaroğlu, *Optics Communications*, 2009, **282**, 2426-2430.
18. F. Y. Ke, C. Zhang, S. Y. Guang and H. Y. Xu, *J Appl Polym Sci*, 2013, **127**, 2628-2634.
19. P. Andre, G. Cheng, A. Ruseckas, T. van Mourik, H. Fruchtl, J. A. Crayston, R. E. Morris, D. Cole-Hamilton and I. D. Samuel, *J. Phys. Chem. B*, 2008, **112**, 16382-16392.
20. P. Chen, X. Huang, Q. Zhang, K. Xi and X. Jia, *Polymer*, 2013, **54**, 1091-1097.
21. D.-G. Kim, H.-S. Sohn, S.-K. Kim, A. Lee and J.-C. Lee, *Journal of Polymer Science Part A: Polymer Chemistry*, 2012, **50**, 3618-3627.
22. Z. Yan, H. Xu, S. Guang, X. Zhao, W. Fan and X. Y. Liu, *Advanced Functional Materials*, 2012, **22**, 345-352.
23. H. B. Fan, J. Y. He and R. J. Yang, *J Appl Polym Sci*,

2013, **127**, 463-470.
24. M. Liras, M. Pintado-Sierra, F. Amat-Guerri and R. Sastre, *Journal of Materials Chemistry*, 2011, **21**, 12803.
25. X. Su, S. Guang, C. Li, H. Xu, X. Liu, X. Wang and Y. Song, *Macromolecules*, 2010, **43**, 2840-2845.
26. E. Lucenti, C. Botta, E. Cariati, S. Righetto, M. Scarpellini, E. Tordin and R. Ugo, *Dyes and Pigments*, 2013, **96**, 748-755.
27. K. Y. Pu, K. Li, X. Zhang and B. Liu, *Adv. Mater.*, 2010, **22**, 4186-4189.
28. X. Wang, S. Y. Guang, H. Y. Xu, X. Y. Su and N. B. Lin, *Journal Of Materials Chemistry*, 2011, **21**, 12941-12948.
29. F. Alves and I. Nischang, *Chemistry-A European Journal*, 2013, **19**, 17310-17313.
30. E. Gungor, C. Bilir, H. Durmaz, G. Hizal and U. Tunca, *Journal of Polymer Science Part A: Polymer Chemistry*, 2009, **47**, 5947-5953.
31. X. Wang, Y. Yang, P. Gao, D. Li, F. Yang, H. Shen, H. Guo, F. Xu and D. Wu, *Chemical communications*, 2014, **50**, 6126-6129.
32. M. Y. Lo, K. Ueno, H. Tanabe and A. Sellinger, *Chem. Rec.*, 2006, **6**, 157-168.
33. G. Zhang, G. Yang, S. Wang, Q. Chen and J. S. Ma, *Chemistry*, 2007, **13**, 3630-3635.
34. Y. K. Zhu, S. Y. Guang and H. Y. Xu, *Chinese Chemical Letters*, 2012, **23**, 1095-1098.
35. D. Clarke, S. Mathew, J. Matisons, G. Simon and B. W. Skelton, *Dyes and Pigments*, 2012, **92**, 659-667.
36. X. Su, H. Xu, Y. Deng, J. Li, W. Zhang and P. Wang, *Materials Letters*, 2008, **62**, 3818-3820.
37. H. Xu, B. Yang, X. Gao, C. Li and S. Guang, *J Appl Polym Sci*, 2006, **101**, 3730-3735.
38. E. Arunkumar, C. C. Forbes, B. C. Noll and B. D. Smith, *J. AM. CHEM. SOC.*, 2005, **127**, 3288-3289.
39. X. Lu, Z. Guo, C. Sun, H. Tian and W. Zhu, *J. Phys. Chem. B*, 2011, **115**, 10871-10876.